

Return Augmented Decision Transformer for Off-Dynamics Reinforcement Learning

Ruhan Wang^{*‡} Yu Yang^{†‡} Zhishuai Liu[§] Dongruo Zhou[¶] Pan Xu^{||}

November 1, 2024

Abstract

We study offline off-dynamics reinforcement learning (RL) to utilize data from an easily accessible source domain to enhance policy learning in a target domain with limited data. Our approach centers on return-conditioned supervised learning (RCSL), particularly focusing on the decision transformer (DT), which can predict actions conditioned on desired return guidance and complete trajectory history. Previous works tackle the dynamics shift problem by augmenting the reward in the trajectory from the source domain to match the optimal trajectory in the target domain. However, this strategy can not be directly applicable in RCSL owing to (1) the unique form of the RCSL policy class, which explicitly depends on the return, and (2) the absence of a straightforward representation of the optimal trajectory distribution. We propose the Return Augmented Decision Transformer (RADT) method, where we augment the return in the source domain by aligning its distribution with that in the target domain. We provide the theoretical analysis demonstrating that the RCSL policy learned from RADT achieves the same level of suboptimality as would be obtained without a dynamics shift. We introduce two practical implementations RADT-DARA and RADT-MV respectively. Extensive experiments conducted on D4RL datasets reveal that our methods generally outperform dynamic programming based methods in off-dynamics RL scenarios.

1 Introduction

Off-dynamics reinforcement learning (Eysenbach et al., 2020; Jiang et al., 2021; Liu et al., 2022; Liu and Xu, 2024) is commonly employed in decision-making scenarios such as autonomous driving (Pan et al., 2017) and medical treatment (Laber et al., 2018; Liu et al., 2023), where training the policy through extensive trial-and-error in the real target environment is often costly, unethical, or infeasible. A practical approach involves training the RL policy in source environments with similar dynamics that are easier to simulate or access. However, the dynamic shift between the source and target environments results in a challenging sim-to-real gap, which can lead to catastrophic failures when deploying the policy learned from the source environment to the target environment.

^{*}Indiana University; email: ruhwang@iu.edu

[†]Duke University; email: yu.yang@duke.edu

[‡]Equal contribution

[§]Duke University; email: zhishuai.liu@duke.edu

[¶]Indiana University; email: dz13@iu.edu

^{||}Duke University; email: pan.xu@duke.edu

In addition to the dynamic shift problem, in these practical scenarios, we also often do not have real-time online interactions with the source environment due to constraints in time and computational resources. Therefore, we must learn the policy from a pre-collected dataset generated by some behavior policies. It presents a highly challenging learning task, characterized by its off-policy, offline, and off-dynamics nature. Supervised learning-based methods (Brandfonbrener et al., 2022; Chen et al., 2021) have recently emerged as a promising class of stable and scalable alternatives to conventional offline reinforcement learning algorithms based on dynamic programming (Levine et al., 2020). In the offline off-dynamics setting, the available data to train the policy is primarily collected from the source domain, with only a small fraction coming from the target domain. Our study focuses on leveraging and enhancing the Decision Transformer (DT) (Chen et al., 2021) in off-dynamics reinforcement learning, which can be seen as a special case of return-conditioned supervised learning (RCSL) methods (Brandfonbrener et al., 2022; Emmons et al., 2021). Despite the growing interest in developing DT methods for various reinforcement learning tasks, there has been no explicit effort to address the off-dynamics RL problem.

There are several previous significant works in off-dynamics reinforcement learning that employ reward augmentation to address the dynamics shift between source and target environments (Eysenbach et al., 2020; Liu et al., 2022). In particular, Eysenbach et al. (2020) proposed the DARC algorithm to train a policy in the source domain using augmented rewards. These augmentations are derived by minimizing the KL distance between the distribution of trajectories generated by the learning policy in the source domain and those generated by the optimal policy in the target domain. Liu et al. (2022) extended this idea to the offline setting with the DARA algorithm. However, these reward augmentation techniques for dynamic programming based RL algorithms are not directly applicable to RCSL methods for two primary reasons. First, the policy classes used in RCSL methods explicitly depend on the conditional return-to-go function, leading to different trajectory distributions that invalidate the trajectory matching methods. Second, the augmentation techniques in Eysenbach et al. (2020); Liu et al. (2022) explicitly rely on the form of the optimal trajectory distribution in the target domain. In contrast, there is no straightforward representation of the optimal RCSL policy and the trajectory distribution. Therefore, novel augmentation mechanisms must be derived for RCSL methods to effectively address off-dynamics reinforcement learning.

In this work, we propose the Return Augmented Decision Transformer (RADT) algorithm, which augments the returns of trajectories from the source environment to align with the target environment. Through rigorous analysis, we show that the RCSL policy learned with RADT in the source domain achieves suboptimality comparable to that learned directly in the target domain without dynamics shift. Specifically, **our contributions are summarized as follows:**

- We propose the novel Return Augmented Decision Transformer (RADT) method, which augments the returns of offline trajectories in the source domain using a small portion of data from the target domain. We derive our return augmentation method using reward augmentation from existing dynamic programming based methods and direct return distribution matching respectively, resulting in two practical RADT implementations: RADT-DARA and RADT-MV.
- We provide a rigorous analysis demonstrating that the return-conditioned policy learned from our RADT approach can achieve the same suboptimality level as a policy learned directly from the target domain under standard data coverage assumptions, implying that return augmentation could enhance the performance of RCSL in off-dynamics RL when the available source dataset size is much larger than the available target dataset size.
- We conduct comprehensive experiments on the D4RL benchmark, specifically targeting the Hopper,

Walker2D, and HalfCheetah environments. We create source environments with modifications in BodyMass shift, JointNoise shift, Kinematic shift, and Morphology shift, and then gather data from these modified settings. The policy is trained on this source dataset and evaluated in an unmodified target environment. Our results indicate that DT consistently outperforms baseline algorithms in off-dynamics settings, highlighting DT’s ability to address challenges associated with offline dynamics. Moreover, our newly developed RADT methods build on DT’s capabilities, achieving superior outcomes in most tested configurations.

2 Related Work

Off-dynamics reinforcement learning (RL). It is a type of domain adaptation problem in RL, drawing on concepts from transfer learning (Pan and Yang, 2009). The DARC algorithm (Eysenbach et al., 2020) addresses this domain adaptation challenge in the online setting by proposing a reward augmentation method that matches the optimal trajectory distribution between the source and target domains. Building on this, DARA (Liu et al., 2022) utilizes reward augmentation to supplement a limited target dataset with a larger source dataset. Unlike DARC and DARA, which are based on dynamic programming, our work adopts the adaptation setting of DARA and introduces a novel augmentation method tailored for RCSL, specifically focusing on the Decision Transformer.

Return Conditioned Supervised Learning (RCSL). It is a general framework for powerful supervised methods in offline RL (Brandfonbrener et al., 2022). Notable works such as RvS (Emmons et al., 2021) and Decision Transformer (DT) (Chen et al., 2021) have shown competitive performance compared to traditional RL methods. The core idea of RCSL is to condition policies on a desired return. In this paper, we primarily focus on DT, which is a specific instance of RCSL and conducts offline RL through sequence generation. The generalization potential of DT has inspired researchers to explore its use in various settings. For example, Zheng et al. (2022); Xu et al. (2022) leverage the DT in the offline-to-online RL and meta RL respectively. However, no prior work has explicitly explored the adaptation capabilities of DT in the off-dynamics RL setting.

3 Preliminary

Sequential Decision-Making. We consider a general sequential decision-making problem. At each step t , the agent receives an observation o_t from the environment. Based on the history up to step t , the agent makes action a_t and receives the reward r_t from the environment. The agent interacts with the environment in episodes with a length H . We use $\tau = (o_1, a_1, r_1, \dots, o_H, a_H, r_H)$ to denote a whole trajectory, and we use $g(\tau) = \sum_{t=1}^H r_t$ to denote the cumulative return of the trajectory. We model the environment as a Markov Decision Process (MDP) M , which consists of $(\mathcal{S}, \mathcal{A}, p, r, H)$. Here \mathcal{S} is the state space, each state s represents the possible history up to some time step t , i.e., $s = (o_1, a_1, r_1, \dots, o_t)$. \mathcal{A} is the action space, $p(s'|s, a)$ is the transition dynamic that determines the transition probability for the agent to visit state s' from current state s with the action a . $r(s, a)$ denotes the reward function. We re-define a trajectory as $\tau = (s_1, a_1, r_1, \dots, s_H, a_H, r_H)$. We assume that each s corresponds to one single time step $t = t(s)$, and we denote $g_\pi(s) = \mathbb{E}_{\tau \sim \pi}[g(\tau)|s_1 = s]$. Then the goal of the agent is to learn a policy $\pi : \mathcal{S} \rightarrow \mathcal{A}$ that maximizes the expected accumulated reward $J(\pi) := \mathbb{E}_{\tau \sim \pi}[g(\tau)]$. We denote the optimal policy as π^* .

Offline RL and Decision Transformer. We consider the offline reinforcement learning setting. Given a dataset \mathcal{D} , the goal of the agent is to learn π^* from \mathcal{D} . We assume that the trajectories in

\mathcal{D} are generated from a behavior policy β . In this work, we mainly consider Decision Transformer (DT)(Chen et al., 2021) as our backbone algorithm. DT is a type of sequential modeling technique based on Transformer (Vaswani et al., 2017) to solve offline RL problems. In detail, DT maintains a function $\pi(a|s, g)$ as its policy function. To train the policy π , DT aims to minimize the following negative log-likelihood function $\hat{L}(\pi)$, where

$$\hat{L}(\pi) := - \sum_{\tau \in \mathcal{D}} \sum_{1 \leq t \leq H} \log \pi(a_t | s_t, g(\tau)),$$

To evaluate π , DT defines a *conditioning function* $f : \mathcal{S} \rightarrow \mathbb{R}$, which maps each state to a return value and guides the policy π_f within the environment, where $\pi_f(a|s) := \pi(a|s, f(s))$. The conditioning function is pivotal in DT, as varying $f(s)$ for a given state s results in different policies. To achieve the optimal policy, $f(s)$ should be maximized (Zhuang et al., 2024).

Offline Off-Dynamics RL. In this work, we consider the offline off-dynamics RL problem, where the agent has access to two offline datasets \mathcal{D}^S and \mathcal{D}^T . $\mathcal{D}^S, \mathcal{D}^T$ include the data collected from the *source environment* M^S and the *target environment* M^T . The source and the target environments share the same reward function r , with different transition dynamics p^S and p^T . In practice, we assume that the dataset size from the source dataset $|\mathcal{D}^S|$ is much larger than the data coming from the target dataset $|\mathcal{D}^T|$. Then the agent aims to find the optimal policy for the target environment M^T based on the data from both the source and the target environments. Since the transition dynamic p^S and p^T are different, we can not directly apply existing RL algorithms on the union $\mathcal{D}^S \cup \mathcal{D}^T$.

4 Return Augmentation for Goal Conditioned Supervised Learning

4.1 Return-Augmented Framework

DT has the potential to address offline off-dynamics reinforcement learning challenges, as shown in Table 2. However, it still has certain limitations. To overcome these, we propose a general framework that efficiently learns the optimal policy for the target environment using the combined dataset $\mathcal{D}^S \cup \mathcal{D}^T$. Leveraging the return-conditioning nature of DT, we introduce a *return augmentation* technique that modifies returns in the offline source dataset through a transformation function. This approach allows the policy derived from the augmented source dataset to effectively approximate the optimal policy of the target environment, as illustrated in the following equation, where π^S represents a strong candidate for approximating the optimal policy of the target environment and ψ is the carefully chosen transformation function.

$$\begin{aligned} \pi^S &= \arg \min_{\pi} \hat{L}(\pi) \\ &:= - \sum_{\tau \in \mathcal{D}^S} \sum_{1 \leq t \leq H} \log \pi(a_t | s_t, \psi(g(\tau))). \end{aligned}$$

We call our method *Return Augmented DT (RADT)*. Next we introduce two methods to construct ψ , based on the dynamics-aware reward augmentation (DARA) technique (Eysenbach et al., 2020; Liu et al., 2022), and a direct return distribution matching method.

4.2 Dynamics-Aware Reward Augmentation

We first summarize the idea of dynamics-aware reward augmentation (DARA) (Eysenbach et al., 2020; Liu et al., 2022). Let $p^T(s'|s, a)$ denote the transition dynamic of the target environment, and $p^S(s'|s, a)$ denote the source environment. According to the connection of RL and probabilistic

inference (Levine, 2018), we can turn the optimal policy finding problem into an inference problem. We use O to denote a binary random variable where $O = 1$ suggests τ is a trajectory induced by the optimal policy. Given a trajectory τ , the likelihood of τ being a trajectory induced by the optimal policy under the target environment is $p^T(O = 1|\tau) = \exp(\sum_{t=1}^H r(s_t, a_t)/\eta)$, where η is the step size parameter used for tuning. It means that the trajectory with higher cumulative rewards is more likely to be the trajectory induced by the optimal policy. We introduce a variational distribution $p_\pi^S(\tau) = p(s_1) \prod_{t=1}^T p^S(s_{t+1}|s_t, a_t) \pi(a_t|s_t)$ to approximate $p_\pi^T(O = 1|\tau)$. Then we have

$$\begin{aligned}
& \log p_\pi^T(O = 1) \\
&= \log \mathbb{E}_{\tau \sim p_\pi^T(\tau)} p^T(O = 1|\tau) \\
&\geq \mathbb{E}_{\tau \sim p_\pi^S(\tau)} [\log p^T(O = 1|\tau) + \log (p_\pi^T(\tau)/p_\pi^S(\tau))] \\
&= \mathbb{E}_{\tau \sim p_\pi^S(\tau)} [\sum_{t=1}^T r(s_t, a_t)/\eta - \log (p^S(s_{t+1}|s_t, a_t)/p^T(s_{t+1}|s_t, a_t))]. \tag{4.1}
\end{aligned}$$

Therefore, we obtain an evidence lower bound of $p_\pi^T(O = 1)$, which equals to find a policy to maximize the value in the source environment, with the augmented reward $r^S(s_t, a_t) = r(s_t, a_t) + \eta \log p^T(s_{t+1}|s_t, a_t) - \eta \log p^S(s_{t+1}|s_t, a_t)$. Following Eysenbach et al. (2020), to estimate the $\log p^T(s_{t+1}|s_t, a_t) - \log p^S(s_{t+1}|s_t, a_t)$, we use a pair of learned binary classifiers which infers whether the transitions come from the source or target environments. Specifically, we denote classifiers $q_{sas}(\cdot|s, a, s')$ and $q_{sa}(\cdot|s, a)$, which return the probability for some (s, a, s') or (s, a) tuples whether they belong to the source or the target environments. Then according to Eysenbach et al. (2020), we have

$$\begin{aligned}
& \log p^T(s_{t+1}|s_t, a_t) - \log p^S(s_{t+1}|s_t, a_t) \\
&= \Delta r(s_t, a_t, s_{t+1}) \\
&:= \log \frac{q(M^T|s_t, a_t, s_{t+1})}{q(M^S|s_t, a_t, s_{t+1})} - \log \frac{q_{sa}(M^T|s_t, a_t)}{q_{sa}(M^S|s_t, a_t)}. \tag{4.2}
\end{aligned}$$

For a trajectory $\tau = (s_1, a_1, r_1, \dots, s_H, a_H, r_H)$, we denote the transformation $\psi(g(s_t)) := \sum_{h=t}^H r_h + \eta \sum_{h=t}^H \Delta r(s_h, a_h, s_{h+1})$. We denote such a transformation method as RADT-DARA.

4.3 Direct Matching of Return Distributions

The reward augmentation strategy in RADT-DARA stems from the probabilistic inference view of RL which matches the distribution of the learning trajectory in the source domain with that of the optimal trajectory in the target domain (Eysenbach et al., 2020). However, it does not fully capture the power of DT, which is able to induce a *family of policies* that are conditioned on the return-to-go f . By varying f , DT enables the generation of a diverse range of policies, including the optimal one. In contrast, RADT-DARA assumes a single, fixed target policy, and thus its augmentation strategy cannot generalize across multiple policies induced by varying f in DT. As a result, it cannot find the desired return conditioned policy when evaluated with a different f in the target domain. This motivates us to find a return transformation method ψ to guarantee that $\pi_f^S(a|s) \approx \pi_f^T(a|s)$ for all f .

We consider a simplified case where both D^S and D^T are generated by following the same behavior policy $\beta(a|s)$. We use $d_S(A)$ and $d_T(A)$ to denote the probability for event A to happen under the source and target environments following β . With a slight abuse of notation, we use g_S and g_T to denote the return following the behavior policy. Then we characterize the learned policies by

DT under the infinite data regime (Brandfonbrener et al., 2022) for both the source environment and target environment. According to Brandfonbrener et al. (2022), $\pi_f^S(a|s) = P^S(a|s, \psi(g_S) = f(s))$. Then we can express π^S and π^T as

$$\begin{aligned}\pi_f^S(a|s) &= \frac{d_S(a|s)d_S(\psi(g_S) = f(s)|s, a)}{d_S(\psi(g_S) = f(s)|s)}, \\ \pi_f^T(a|s) &= \frac{d_T(a|s)d_T(g_T = f(s)|s, a)}{d_T(g_T = f(s)|s)}.\end{aligned}$$

Since the behavior policies over the source and target environments are the same, we have $d_S(a|s) = d_T(a|s)$ for all (s, a) . Then in order to guarantee $\pi_f^S(a|s) = \pi_f^T(a|s)$ we only need to guarantee $d_S(\psi(g_S(s)) = \cdot|s, a) = d_T(g_T(s) = \cdot|s, a)$, $\forall s, a$. Denote the cumulative distribution function (CDF) of g^S conditioned on s, a is $g^S|s, a \sim G_\beta^S(s, a)$, and $g^T|s, a \sim G_\beta^T(s, a)$. Then if both $G_\beta^S(s, a)$ and $G_\beta^T(s, a)$ are invertible, we can set ψ as follows

$$\psi(g^S) = G_\beta^{T,-1}(G_\beta^S(g_S; s, a); s, a). \quad (4.3)$$

Remark 4.1. If there exist P^S , P^T , and r such that the DARA-type augmented reward-to-go satisfies (4.3), then the DARA-type reward augmentation can be deemed as a special case of the transformation (4.3).

In general, G_β^T and G_β^S are hard to obtain and computationally intractable, making ψ intractable either. We use Laplace approximation to approximate both G_β^T and G_β^S by Gaussian distributions, e.g., $G_\beta^S(s, a) \sim N(\mu^S(s, a), \sigma_S^2(s, a))$ and $G_\beta^T(s, a) \sim N(\mu^T(s, a), \sigma_T^2(s, a))$. Then it is easy to obtain that

$$\psi(g^S) := \frac{g^S - \mu^S(s, a)}{\sigma^S(s, a)} \cdot \sigma^T(s, a) + \mu^T(s, a). \quad (4.4)$$

We denote DT with a ψ transformation from (4.4) by *RADT-Mean-Variance (RADT-MV)*, since such a transformation only depends on the estimation of mean values μ^S, μ^T and variance σ^S, σ^T .

4.4 Sample Complexity of Off-Dynamics RCSL

In this section, we provide an overview of the sample complexity for off-dynamics RCSL. Let N^S represent the number of trajectories in the source dataset \mathcal{D}^S and N^T the number of trajectories in the target dataset \mathcal{D}^T . We define $J^T(\pi)$ as the expected cumulative reward under any policy π within the target environment. Our theorem is established based on the following assumption.

Assumption 4.2 (Theorem 1, Brandfonbrener et al. 2022). (1) (Return coverage) $P_\beta^T(g = f(s_1)|s_1) \geq \alpha_f$ for all initial states s_1 . (2) (Near determinism) $P(r \neq r(s, a) \text{ or } s' \neq T(s, a)|s, a) \leq \epsilon$ at all s, a for some functions T and r . (3) (Consistency of f) $f(s) = f(s') + r$ for all s .

Assumption 4.3 (Theorem 2, Brandfonbrener et al. 2022). (1) (Bounded occupancy mismatch) $P_{\pi_f^{\text{RCSL}(s)}} \leq C_f P_\beta(s)$ for all s . (2) (Return coverage) $P_\beta^T(g = f(s)|s) \geq \alpha_f$ for all s . (3) (Domain occupancy overlap) $d_\beta^T(s) \leq \gamma_f d_\beta^S(s)$ for all s .

Assumption 4.4 (Corollary 3, Brandfonbrener et al. 2022). (1) The policy class Π is finite. (2) $|\log \pi(a|s, g) - \log \pi(a'|s', g')| \leq c$ for any (a, s, g, a', s', g') and all $\pi \in \Pi$. 3) The approximation error is bounded by ϵ_{approx} , i.e., $\min_{\pi \in \Pi} L(\pi) \leq \epsilon_{\text{approx}}$.

Theorem 4.5. Under Assumption 4.2, Assumption 4.3 and Assumption 4.4 on the coverage of the offline dataset and the occupancy overlap of the source and target environments, with high probability, we have

$$J^T(\pi^*) - J^T(\hat{\pi}_f) = O(1/(N^T + N^S)^{1/4}),$$

where O omits terms that are independent of the sample size N^T of the target domain and the sample size N^S of the source domain.

Remark 4.6. Theorem 4.5 suggests that the modified samples from the source domain could enhance the performance of RCSL, for which the sample complexity is approximately $O((1/N^T)^{1/4})$.

For more theoretical details, please refer to Appendix A.

5 Experiments

Table 1 Performance comparison of algorithms across varying target dataset sizes (**1T** and **10T**) using the Random, Medium, Medium Replay, and Medium Expert datasets in the Walker2D, Hopper, and HalfCheetah environments. Results are averaged over five seeds.

		BEAR		AWR		BCQ	
		10T	1T	10T	1T	10T	1T
Walker2D	Random	4.348 ± 2.443	1.236 ± 0.904	7.400 ± 1.107	3.955 ± 4.352	5.498 ± 2.888	5.482 ± 0.497
	Medium	13.143 ± 3.016	4.638 ± 3.882	78.060 ± 0.772	68.023 ± 1.687	74.735 ± 1.184	62.567 ± 2.459
	Medium Replay	5.852 ± 0.168	0.777 ± 0.105	58.286 ± 1.684	28.426 ± 2.974	64.735 ± 2.555	62.567 ± 0.683
	Medium Expert	21.383 ± 1.237	9.267 ± 1.692	109.154 ± 0.976	100.566 ± 0.513	101.840 ± 1.962	101.610 ± 1.309
Hopper	Random	3.232 ± 1.534	5.179 ± 2.711	7.902 ± 1.474	6.394 ± 1.006	9.243 ± 0.662	2.352 ± 1.372
	Medium	20.398 ± 2.102	8.770 ± 0.402	64.494 ± 2.217	55.269 ± 2.254	73.462 ± 2.527	63.308 ± 0.418
	Medium Replay	5.554 ± 0.842	5.264 ± 0.283	57.548 ± 1.778	54.259 ± 1.295	60.385 ± 0.418	68.448 ± 0.251
	Medium Expert	88.236 ± 2.192	31.968 ± 1.213	105.361 ± 1.392	54.098 ± 1.165	102.775 ± 1.912	62.287 ± 1.689
HalfCheetah	Random	29.320 ± 0.325	22.133 ± 0.150	2.396 ± 0.130	2.477 ± 0.051	2.249 ± 0.010	2.249 ± 0.001
	Medium	10.657 ± 0.271	2.659 ± 0.167	42.209 ± 0.611	41.672 ± 0.732	46.188 ± 0.423	41.051 ± 2.908
	Medium Replay	19.588 ± 0.453	1.602 ± 0.275	41.041 ± 0.729	28.023 ± 4.027	38.575 ± 2.060	25.828 ± 6.142
	Medium Expert	16.160 ± 0.208	3.089 ± 0.104	90.212 ± 2.259	901.68 ± 1.398	95.535 ± 4.042	60.173 ± 4.175
Walker2D	Random	5.498 ± 0.851	5.485 ± 2.861	6.111 ± 0.257	3.183 ± 0.596	7.415 ± 4.824	5.162 ± 3.619
	Medium	78.191 ± 1.839	65.618 ± 2.818	22.261 ± 2.811	20.953 ± 2.715	79.697 ± 3.348	67.261 ± 2.316
	Medium Replay	80.145 ± 2.286	57.402 ± 6.161	18.529 ± 1.760	20.313 ± 3.488	68.528 ± 1.924	34.482 ± 5.890
	Medium Expert	101.840 ± 0.467	101.611 ± 0.143	21.196 ± 3.103	20.569 ± 0.983	108.622 ± 1.815	107.171 ± 1.611
Hopper	Random	8.983 ± 0.398	8.946 ± 3.859	9.871 ± 0.446	4.204 ± 2.895	31.241 ± 3.549	7.794 ± 1.196
	Medium	82.945 ± 0.323	74.489 ± 1.061	32.769 ± 1.788	31.038 ± 2.868	85.589 ± 5.311	66.073 ± 1.745
	Medium Replay	73.168 ± 2.712	71.401 ± 2.106	8.638 ± 1.395	5.849 ± 0.146	69.701 ± 5.317	61.686 ± 2.592
	Medium Expert	102.071 ± 1.759	82.071 ± 0.483	36.161 ± 2.204	35.099 ± 1.212	108.087 ± 1.049	100.719 ± 1.679
HalfCheetah	Random	25.597 ± 0.054	2.371 ± 0.085	31.308 ± 0.875	23.641 ± 0.569	2.216 ± 0.022	1.158 ± 0.125
	Medium	49.382 ± 0.338	44.393 ± 0.263	65.863 ± 1.289	64.329 ± 2.096	42.273 ± 0.379	41.204 ± 0.430
	Medium Replay	46.966 ± 0.372	26.955 ± 1.274	59.724 ± 1.056	12.277 ± 1.953	34.508 ± 1.482	15.164 ± 4.847
	Medium Expert	87.683 ± 7.753	61.621 ± 13.093	28.221 ± 6.078	25.055 ± 7.834	82.844 ± 7.635	77.500 ± 3.323

In this section, we first outline the fundamental setup of the experiment. We then describe experiments designed to address specific questions, with each question and its corresponding answer detailed in a separate subsection.

- How effective is the Decision Transformer in addressing off-dynamics RL problems?
- What techniques can be applied to enhance the performance of the Decision Transformer in off-dynamics RL scenarios?
- How does the performance of Decision Transformer-based methods compare with other approaches in solving off-dynamics RL problems?

5.1 Basic Experiment Setting

Table 2 Performance Comparison of Algorithms on the Walker2D, Hopper, and HalfCheetah environments under BodyMass and JointNoise Distribution Shifts Using the Medium **1T10S** Dataset. The **1T10S** dataset includes a **1T** (target) dataset alongside a **10S** (source) dataset. Here, "**D-XX**" represents the DARA-augmented variant of the '**XX**' algorithm. Results are averaged across five seeds, with best-performing algorithms highlighted in **blue**. Due to space constraints, additional results for random, medium replay, and medium expert datasets are provided in [Appendix D](#).

Shift	Environment	BEAR	D-BEAR	AWR	D-AWR	BCQ	D-BCQ	CQL	D-CQL	MOPO	D-MOPO	DT
BodyMass	Walker2D	5.776 \pm 1.653	6.516 \pm 3.220	77.442 \pm 0.340	78.004 \pm 0.911	70.681 \pm 0.539	72.023 \pm 0.695	73.317 \pm 1.368	74.276 \pm 2.582	21.617 \pm 1.277	21.621 \pm 1.063	78.768 \pm 1.233
	Hopper	22.436 \pm 0.103	25.608 \pm 1.063	25.843 \pm 0.325	26.594 \pm 1.267	24.853 \pm 1.615	26.487 \pm 1.366	49.094 \pm 2.207	45.101 \pm 0.342	20.765 \pm 3.350	21.495 \pm 0.848	34.057 \pm 0.177
	HalfCheetah	5.431 \pm 1.518	6.009 \pm 1.705	42.293 \pm 0.862	41.800 \pm 0.830	39.835 \pm 0.427	39.333 \pm 0.506	37.081 \pm 0.358	37.189 \pm 0.218	58.457 \pm 1.449	59.311 \pm 0.949	46.954 \pm 0.260
JointNoise	Walker2D	4.926 \pm 1.418	6.933 \pm 1.884	67.636 \pm 1.468	64.303 \pm 0.513	62.696 \pm 1.307	60.681 \pm 1.118	68.962 \pm 0.865	69.141 \pm 0.944	23.552 \pm 1.063	23.574 \pm 0.665	71.068 \pm 1.022
	Hopper	8.536 \pm 1.965	10.576 \pm 2.052	57.021 \pm 0.938	61.463 \pm 0.702	74.559 \pm 0.605	74.853 \pm 0.626	71.495 \pm 0.126	63.611 \pm 1.136	23.556 \pm 1.327	24.992 \pm 0.944	70.685 \pm 0.726
	HalfCheetah	1.948 \pm 1.058	2.901 \pm 0.402	41.992 \pm 0.762	42.545 \pm 0.731	50.511 \pm 0.371	52.149 \pm 0.457	49.046 \pm 0.420	49.284 \pm 0.570	61.073 \pm 0.315	61.447 \pm 0.734	47.725 \pm 0.431

Tasks and Environments. We study established D4RL tasks in the Gym-MuJoCo environment (Fu et al., 2020), a suite built atop the MuJoCo physics simulator, featuring tasks such as locomotion and manipulation. Particularly, we focused on three environments: Walker2D, Hopper, and HalfCheetah.

In tackling the off-dynamics reinforcement learning problem, we differentiate between the **Source** and the **Target** environments. The Target environment is based on the original Gym-MuJoCo framework, whereas the Source environment is constructed using the following methods. For further details on the source environment, please refer to the [Appendix C](#).

- **BodyMass Shift:** Change the mass of the body in the source environment.
- **JointNoise Shift:** Add a noise (randomly sampling in $[-0.05, +0.05]$) to the actions.
- **Kinematic Shift:**
 - **Walker2D Environment:** The rotation range of the joint on the right leg’s foot is modified from $[-45, 45]$ to $[-0.45, 0.45]$.
 - **Hopper Environment:**
 - * The rotation range of the joint on the head is adjusted from $[-150, 0]$ to $[-0.15, 0]$.
 - * The rotation range of the joint on the foot is changed from $[-45, 45]$ to $[-18, 18]$.
 - **HalfCheetah Environment:** The rotation range of the joint on the back leg’s thigh is modified from $[-0.52, 1.05]$ to $[-0.0052, 0.0105]$.
- **Morphology Shift:** In the Walker2D environment, we adjust the size of the right leg’s thigh. In the Hopper environment, we modify the size of the head. In HalfCheetah, we alter the size of both thighs.

Dataset. For the Target Dataset corresponding to the Target Environment, we leverage the official D4RL data to construct two datasets: 10T and 1T. The 10T dataset comprises ten times

the number of trajectories compared to the 1T dataset. ¹ For the Source Dataset collection, we begin by modifying the environment through adjustments to the XML file of the MuJoCo simulator. We then collect the Random, Medium, Medium-Replay, and MediumExpert offline datasets in the modified environments, following the same data collection procedure as used in D4RL. For further details on the dataset collection process and the datasets, please refer to the [Appendix C](#).

Baselines. In selecting our baseline models, we incorporate a diverse set of well-established off-dynamics RL methods, including BEAR (Kumar et al., 2019), AWR (Peng et al., 2019), BCQ (Fujimoto et al., 2019), CQL (Kumar et al., 2020), and MOPO (Yu et al., 2020). Furthermore, we enhance these baseline models by incorporating DARA augmentation, resulting in augmented algorithms that also serve as baselines for comparison with our proposed method. In establishing hyperparameters, we ensure consistency across tasks for certain parameters, such as the learning rate and the number of iteration steps. Refer to the [Appendix C](#) for further details on the parameter settings.

Table 3 Performance Comparison of DT and RADT Algorithms in Walker2D and Hopper Environments. This table presents the averaged results over five seeds for Decision Transformers trained on the **10T**, **1T**, and **1T10S** datasets (denoted as **10T-DT**, **1T-DT**, **1T10S-DT**), along with **RADT-MV** and **RADT-DARA**, across random, medium, medium-replay, and medium-expert datasets. The best-performing algorithms among **1T10S-DT**, **RADT-DARA**, and **RADT-MV** are highlighted in **blue**. \uparrow indicates scenarios where RADT algorithm outperforms DT on the mixed dataset **1T10S**, and \downarrow shows where it underperforms.

Shift	Walker2D Random					Walker2D Medium				
	10T-DT	1T-DT	1T10S-DT	RADT-MV	RADT-DARA	10T-DT	1T-DT	1T10S-DT	RADT-MV	RADT-DARA
BodyMass	7.415 \pm (4.824)	5.162 \pm (3.619)	6.571 \pm (4.824)	7.318 \pm (0.098) \uparrow	7.734 \pm (2.886) \uparrow	79.697 \pm (3.348)	67.261 \pm (2.316)	78.768 \pm (1.233)	80.857 \pm (1.715) \uparrow	78.257 \pm (2.423) \downarrow
JointNoise			6.236 \pm (5.720)	7.657 \pm (0.919) \uparrow	6.075 \pm (1.914) \downarrow			71.068 \pm (1.022)	72.651 \pm (1.834) \uparrow	71.779 \pm (1.706) \uparrow
Shift	Walker2D Medium Replay					Walker2D Medium Expert				
	10T-DT	1T-DT	1T10S-DT	RADT-MV	RADT-DARA	10T-DT	1T-DT	1T10S-DT	RADT-MV	RADT-DARA
BodyMass	68.528 \pm (1.924)	34.482 \pm (5.890)	73.664 \pm (1.920)	73.708 \pm (1.570) \uparrow	67.565 \pm (0.799) \downarrow	108.622 \pm (1.815)	107.171 \pm (1.611)	84.430 \pm (0.823)	88.235 \pm (1.886) \uparrow	85.328 \pm (0.865) \uparrow
JointNoise			58.255 \pm (3.181)	55.722 \pm (2.653) \downarrow	62.226 \pm (0.383) \uparrow			115.746 \pm (1.116)	111.06 \pm (2.247) \downarrow	111.236 \pm (0.914) \downarrow
Shift	Hopper Random					Hopper Medium				
	10T-DT	1T-DT	1T10S-DT	RADT-MV	RADT-DARA	10T-DT	1T-DT	1T10S-DT	RADT-MV	RADT-DARA
BodyMass	31.241 \pm (3.549)	7.794 \pm (1.196)	8.746 \pm (0.554)	9.668 \pm (0.054) \uparrow	8.467 \pm (1.196) \downarrow	85.589 \pm (5.311)	66.073 \pm (1.745)	34.057 \pm (0.177)	39.435 \pm (1.239) \uparrow	37.787 \pm (1.914) \uparrow
JointNoise			6.236 \pm (1.552)	7.524 \pm (0.656) \uparrow	7.842 \pm (0.149) \uparrow			70.685 \pm (0.726)	70.356 \pm (3.657) \downarrow	78.325 \pm (2.522) \uparrow
Shift	Hopper Medium Replay					Hopper Medium Expert				
	10T-DT	1T-DT	1T10S-DT	RADT-MV	RADT-DARA	10T-DT	1T-DT	1T10S-DT	RADT-MV	RADT-DARA
BodyMass	69.701 \pm (5.317)	61.686 \pm (2.592)	64.216 \pm (1.504)	66.092 \pm (0.233) \uparrow	60.393 \pm (1.086) \downarrow	108.087 \pm (1.049)	100.719 \pm (1.679)	33.554 \pm (0.846)	52.873 \pm (0.454) \uparrow	33.631 \pm (1.605) \uparrow
JointNoise			61.870 \pm (0.249)	77.825 \pm (1.638) \uparrow	83.525 \pm (1.728) \uparrow			108.254 \pm (1.583)	109.367 \pm (1.084) \uparrow	108.261 \pm (2.612) \uparrow
Shift	HalfCheetah Random					HalfCheetah Medium				
	10T-DT	1T-DT	1T10S-DT	RADT-MV	RADT-DARA	10T-DT	1T-DT	1T10S-DT	RADT-MV	RADT-DARA
BodyMass	2.216 \pm (0.022)	1.158 \pm (0.125)	2.205 \pm (0.014)	2.220 \pm (0.021) \uparrow	2.209 \pm (0.018) \uparrow	42.273 \pm (0.379)	41.204 \pm (0.430)	39.954 \pm (0.260)	40.250 \pm (0.911) \uparrow	37.599 \pm (0.395) \downarrow
JointNoise			2.215 \pm (0.011)	2.206 \pm (0.015) \downarrow	2.210 \pm (0.014) \downarrow			47.725 \pm (0.431)	44.149 \pm (3.672) \downarrow	47.833 \pm (0.284) \uparrow
Shift	HalfCheetah Medium Replay					HalfCheetah Medium Expert				
	10T-DT	1T-DT	1T10S-DT	RADT-MV	RADT-DARA	10T-DT	1T-DT	1T10S-DT	RADT-MV	RADT-DARA
BodyMass	34.508 \pm (1.482)	15.164 \pm (4.847)	20.966 \pm (9.607)	27.812 \pm (3.256) \uparrow	24.059 \pm (2.271) \uparrow	82.844 \pm (7.635)	77.500 \pm (3.323)	54.981 \pm (1.147)	56.228 \pm (2.930) \uparrow	51.357 \pm (8.231) \downarrow
JointNoise			36.509 \pm (4.414)	38.417 \pm (4.068) \uparrow	38.031 \pm (3.529) \uparrow			70.573 \pm (8.599)	77.762 \pm (2.099) \uparrow	77.751 \pm (2.702) \uparrow

5.2 Decision Transformer in Off-dynamics Reinforcement Learning

To assess the effectiveness of DT in off-dynamics reinforcement learning scenarios, we first train the DT model on a source dataset and subsequently evaluate its performance in a target environment.

¹Unlike the approach in Liu et al. (2022) which takes both the 10T dataset and 1T dataset as the last 1 million and 100,000 steps of a large offline dataset collected by a predefined policy, our approach uniformly takes steps and trajectories from the dataset to preserve the data diversity.

The results are then compared against other off-dynamics RL methods, including their respective DARA-augmented variants.

To examine the influence of dataset size and quality on DT performance, we evaluated DT using two datasets: 1T and 10T, and compared the outcomes with those of other off-dynamics RL methods. [Table 1](#) provides the experimental results. These findings clearly illustrate that dataset size is a pivotal factor in determining algorithm performance. Insufficient training data substantially limits the algorithm’s capabilities, resulting in diminished performance.

In Off-Dynamics Offline Reinforcement Learning, we utilize a small subset of the target dataset in conjunction with a larger source dataset, rather than relying solely on an extensive target dataset. To assess the ability of algorithms to effectively leverage the source data, we constructed the 1T10S dataset, which integrates a subset of target data (1T) with the complete source dataset (10S). This combined dataset serves as the basis for training various algorithms, followed by their performance evaluation within the target environment. Moreover, recognizing DARA as a potent augmentation technique for enhancing off-dynamics algorithms, we also evaluate the performance of DARA-augmented variants. [Table 2](#) provides a comparative analysis on the 1T10S dataset. The results underscore DT’s effectiveness in handling the complexities of Off-Dynamics Offline Reinforcement Learning.

Although DT demonstrates superior utilization of the source dataset compared to other algorithms, it still exhibits a performance gap when compared to those leveraging a substantial amount of target data (10T). In particular, when there is a substantial divergence between the source and target environments, the performance of the DT on the 1T10S dataset is inferior to its performance on the 1T dataset. Similar to [Bhargava et al. \(2024\)](#), DT’s performance depends on the quality of the offline dataset, especially with the expert data in the offline dataset. The target dataset includes more inferior data from the source dataset would hurt the performance of DT, leading to 1T10S dataset with inferior performance than 1T dataset. To mitigate this gap, we propose two Return-Augmented approaches, RADT-DARA and RADT-MV, aimed at enhancing DT’s efficacy in overcoming the challenges of off-dynamics offline reinforcement learning.

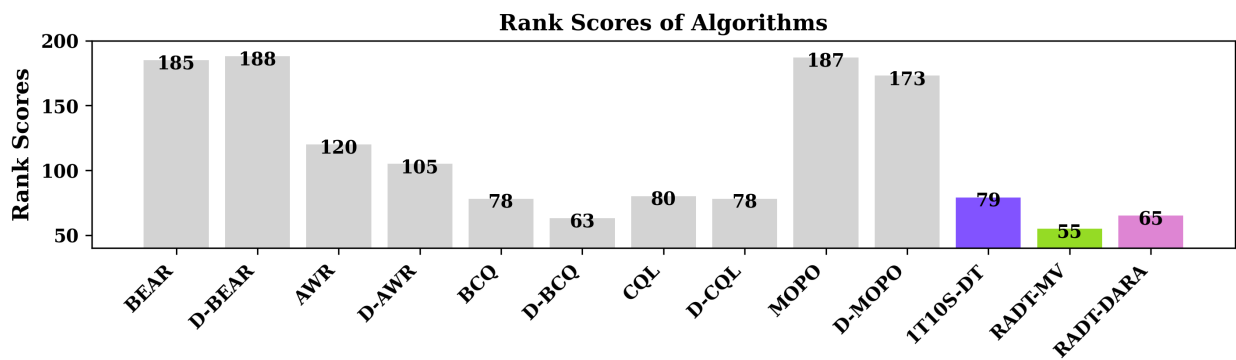


Figure 1 Rank scores for all baseline algorithms and our methods across the Random, Medium, Medium-R, and Medium-E datasets under BodyMass and JointNoise shift settings in the Walker2D, Hopper, and HalfCheetah environments. Ranks were assigned within each dataset, with the highest-performing algorithm receiving rank 1, followed by rank 2, and so on. In cases of tied scores, algorithms were assigned the same rank, and subsequent ranks were adjusted accordingly. Lower rank scores indicate better overall performance.

5.3 RADT for Off-Dynamics RL

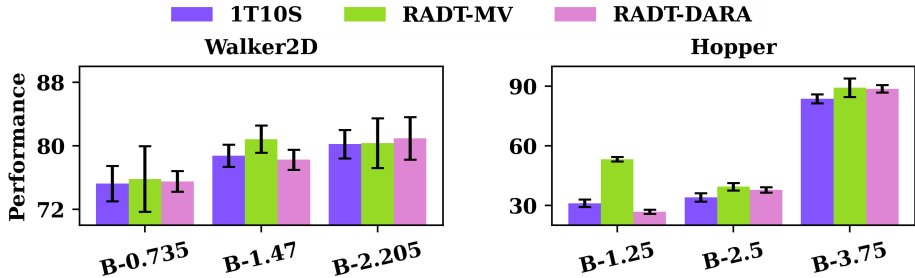


Figure 2 Performance of RADT methods under varying BodyMass shift settings in the Walker2D Medium and Hopper Medium environments. "B-x" denotes that the body mass in the simulator is set to x. The target body mass is 2.94 in the Walker2D environment and 5 in the Hopper environment.

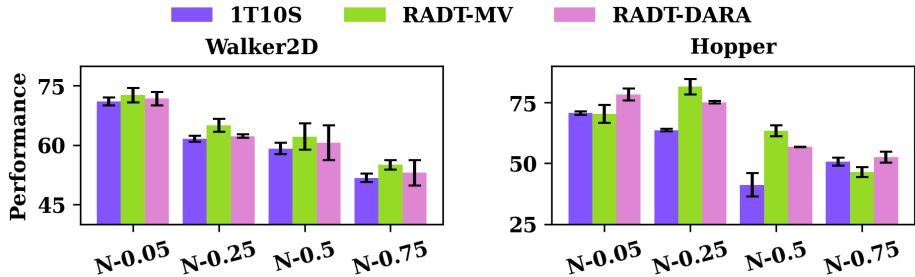


Figure 3 Performance of RADT methods across varying JointNoise shift settings in the Walker2D and Hopper Medium environments. "N-x" denotes the addition of random noise in the range (-x, +x) to the action.

Here we discuss how to implement RADT-DARA and RADT-MV in practice. We implement RADT-DARA based on the dynamic-aware reward augmentation method proposed in Liu et al. (2022). For RADT-MV, it involves training the CQL model across both the Target and Source Environments to derive the respective value functions, denoted as Q_T and Q_S . The derived value functions are then used to relabel the returns of trajectories in the original dataset. More specifically, the relabeled return \hat{g}^S is calculated as defined in (4.4). Within this framework, we use $\mu^S(s, a)$ to denote $Q_S(s, a)$, and $Q_T(s, a)$ corresponds to $\mu^T(s, a)$. For the computation of $\sigma_S(s, a)$ and $\sigma_T(s, a)$, we employ the following methodology: For a given state s , we use the policy of CQL on the source dataset to obtain n available actions $\{a_1^S, a_2^S, \dots, a_n^S\}$ given the state s , with the corresponding Q values $\{Q_S(s, a_1^S), Q_S(s, a_2^S), \dots, Q_S(s, a_n^S)\}$, and n available actions $\{a_1^T, a_2^T, \dots, a_n^T\}$ in the target environment obtained from the CQL policy trained over the target dataset, with the corresponding Q values $\{Q_T(s, a_1^T), Q_T(s, a_2^T), \dots, Q_T(s, a_n^T)\}$. The standard deviations $\sigma_S(s, a)$ and $\sigma_T(s, a)$ are then calculated as specified as follows.

$$\begin{aligned} \sigma_S(s, a) &= \text{std}(Q_S(s, a_1^S), Q_S(s, a_2^S), \dots, Q_S(s, a_n^S)), \\ \sigma_T(s, a) &= \text{std}(Q_T(s, a_1^T), Q_T(s, a_2^T), \dots, Q_T(s, a_n^T)). \end{aligned}$$

For the detailed discussion of this method, please see Section 4. Recall that in (4.4), we need to calculate the ratio $\frac{\sigma_T(s, a)}{\sigma_S(s, a)}$. We introduce a clipping technique to avoid the instability issue caused by extremely large or small $\frac{\sigma_T(s, a)}{\sigma_S(s, a)}$. In detail, we clip $\frac{\sigma_T(s, a)}{\sigma_S(s, a)}$ with an upper bound θ_1 and lower bound θ_2 . We later show that such a trick helps to improve the performance of RADT-MV. Ultimately,

the relabeled Source Dataset is combined with a selected subset of the Target Dataset to create the training dataset for DT.

Table 3 provides a performance comparison between RADT methods and other baselines across the Random, Medium, Medium Replay, and Medium Expert settings in the Walker2D, Hopper and HalfCheetah environments, under BodyMass and JointNoise shift conditions. The results clearly demonstrate that the proposed Return-Augmented methods significantly outperform the baseline approaches. Notably, RADT-MV consistently outperforms RADT-DARA in most scenarios. To facilitate an intuitive comparison, we compute a rank score for each algorithm, assigning ranks within each dataset: the top-performing algorithm receives rank 1, the second-best rank 2, and so forth. In cases of tied scores, algorithms receive the same rank, with subsequent ranks adjusted accordingly. Each algorithm’s final rank score is obtained by summing its ranks across all datasets, with lower average rank scores indicating superior performance. Figure 1 displays the rank scores for all algorithms, illustrating that the proposed RADT methods outperform others in most cases. For additional details on experimental results, please refer to Table 10.

5.4 Ablation Study

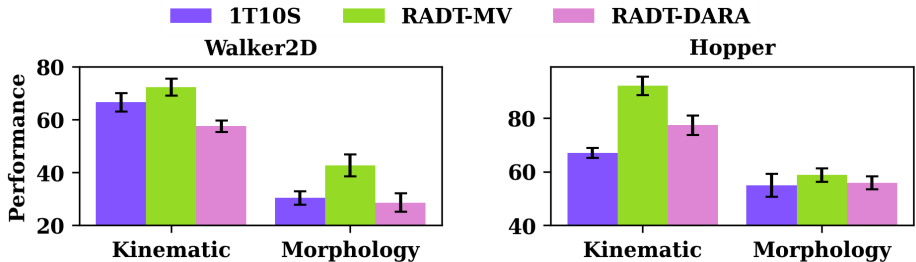


Figure 4 Performance of RADT methods across Kinematic and Morphology Shift settings in the Medium Walker2D and Medium Hopper environments. For more details about these new shift settings, please refer to Section 5.1.

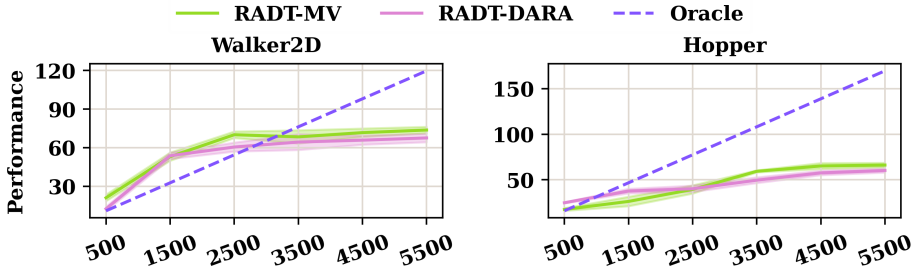


Figure 5 Performance of RADT-MV under varying target return settings in the Walker2D and Hopper Medium Replay environments with the BodyMass Shift setting. The x-axis represents the target return values, the y-axis represents the normalized return. The dash line represents the line $y = x$.

In this section, we present an ablation study to identify the key factors affecting RADT algorithm performance. Most results are provided for the Walker2D and Hopper environments, with additional ablation studies in the HalfCheetah environment available in Appendix D. This study aims to address the following research questions.

- How do RADT methods perform under more significantly shifted source environments?

- How does the target return setting influence the performance of RADT methods?
- How does the clipping technique in RADT-MV impact its performance?
- How does consistency impact the performance of RADT-MV?
- What is the influence of the value function on RADT-MV performance?

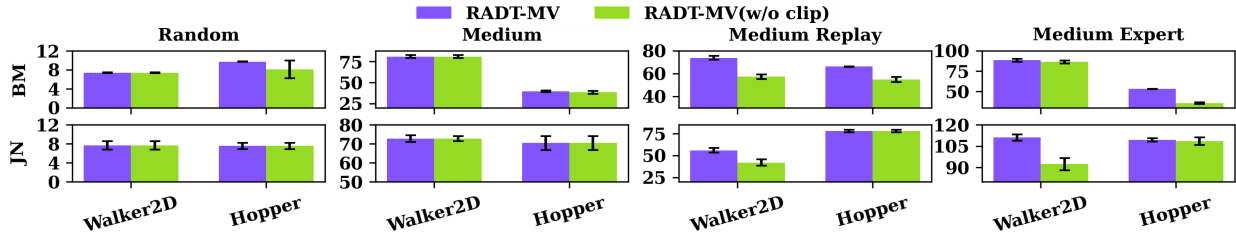


Figure 6 Comparison of RADT-MV with RADT-MV without the clipping technique across Random, Medium, Medium Replay, and Medium Expert settings in the Walker2D, Hopper environments under BodyMass and JointNoise shifts. For detailed experimental settings, refer to the [Appendix C](#).

Algorithm 1 Consistent Return

Require: Trajectories dataset \mathcal{T} , context length K

```

1: Initialize  $\mathcal{T}^K \leftarrow \emptyset$ 
2: for  $\tau \in \mathcal{T}$  do
3:   for  $t = 1, \dots, T - K$  do
4:      $\tau^t \leftarrow \{\tau.s_t, \tau.a_t, \tau.r_t, \dots, \tau.s_{t+K}, \tau.a_{t+K}, \tau.r_{t+K}\}$ 
5:      $\tau^t.R_{t+K} \leftarrow \tau.R_{t+K}$ 
6:     for  $i = t + K - 1, \dots, t$  do
7:        $\tau^t.R_i \leftarrow \tau.r_i + \tau^t.R_{i+1}$ 
8:     end for
9:      $\mathcal{T}^K \leftarrow \mathcal{T}^K \cup \{\tau^t\}$ 
10:  end for
11: end for

```

Ensure: Sliced trajectories dataset \mathcal{T}^K

To investigate the impact of shifting source environments on RADT methods, we evaluated their performance under various BodyMass shift settings, JointNoise settings, Kinematic shifts, and Morphology shifts. The experimental results are presented in [Figures 2, 3, and 4](#). From the experiments, we observed that as the body mass shift increases, creating a larger disparity with the target environment, the performance in both the Walker2D and Hopper Medium environments deteriorates. As more noise is added to the actions, performance decreases in both the Walker2D medium and Hopper medium environments, indicating that random noise in the actions increases the likelihood of failure, leading to worse performance as the noise level rises. In the kinematic shift setting, we modify the Walker2D simulator by removing the right thigh and enlarge the head in the Hopper simulator. In the morphology shift setting, we simulate a broken right foot in the Walker2D environment and break a joint in the Hopper simulator. Across all shifting experiments, RADT-MV consistently achieves better performance than RADT-DARA, with the performance gap being particularly pronounced in larger shift settings, such as kinematic and morphology shifts.

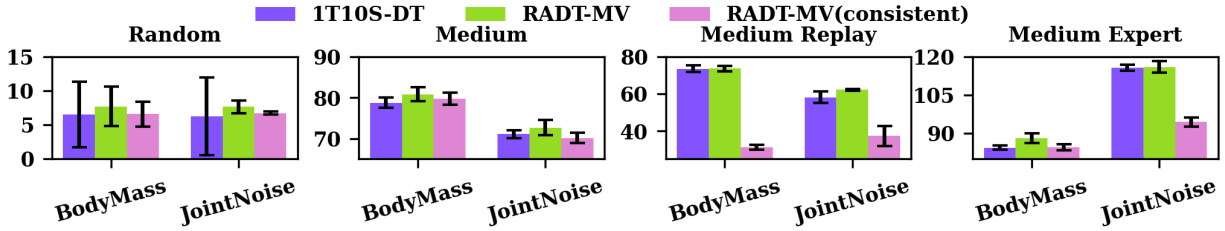


Figure 7 Averaged performance comparison of the 1T10S-DT, RADT-MV, and RADT-MV (consistent) algorithms in the Walker2D environment under BodyMass and JointNoise shift settings. Results are averaged across five random seeds.

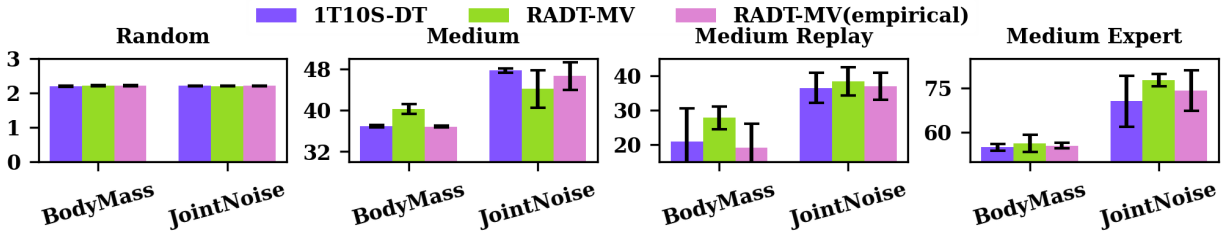


Figure 8 Averaged performance comparison of the 1T10S-DT, RADT-MV, and RADT-MV (empirical) algorithms in the HalfCheetah environment under BodyMass and JointNoise shift settings. Results are averaged across five random seeds.

Setting a large target return is beneficial for maximizing the return in return-based offline reinforcement learning algorithms. We also explore the significance of target return settings in RADT methods within the Medium Replay Walker2D and Hopper environments under BodyMass shift setting. Figure 5 illustrates the performance of RADT methods under different target return settings. From the experimental results, we observe that larger target return settings lead to better performance for RADT methods, with RADT-MV outperforming RADT-DARA.

In RADT-MV, we apply a clipping technique to prevent the appearance of extreme values. We examine the significance of this technique by comparing the performance of RADT-MV with and without clipping in the Medium Walker2D, Hopper, and Halfcheetah settings under BodyMass and JointNoise shifts. Figure 6 presents the results. The results suggest that, in most cases, mitigating the occurrence of extreme values enhances the performance of RADT-MV. Meanwhile, there are instances where RADT-MV remains unaffected by extreme values. That is due to the fact that the original ratio value is already good enough and it does not need additional clipping.

The input sequence in the DT framework maintains consistency, specifically, $R_{t+1} - R_t = r_t$. However, applying RADT-MV to relabel the return in the original sequence may disrupt this consistency. To assess whether this inconsistency affects the performance of RADT-MV, we conduct ablation studies. Specifically, we use an alternative algorithm to relabel the RADT-MV augmented data before slicing the trajectory for input into the DT, as detailed in Algorithm 1. The results, illustrated in Figure 7, demonstrate that RADT-MV significantly outperforms its consistency-enforced variant, particularly in the medium replay environment setting. This outcome suggests that maintaining consistency does not necessarily enhance performance; rather, it may impair the efficacy of the RADT-MV approach within the framework of off-dynamics offline reinforcement learning. This impairment can be attributed to specific dynamics introduced by the RADT-MV method. Specifically, RADT-MV’s relabeling of returns in the original dataset—before using the augmented

dataset to train the DT framework—introduces a critical stitching capability. If consistency is enforced, this stitching capability may be compromised. This issue becomes particularly pronounced in the replay dataset, where data distribution is discrete and the stitching ability of the DT is crucial for performance.

In our approach, the estimated mean and variance is obtained by the CQL policy. We sample the multiple actions $\{a_1^S, a_2^S, \dots, a_n^S\}$ from the current state s with the CQL policy learned in the source dataset to get an estimation of the return mean and variance and similar to the estimation on the target set. To verify the effect of this design, we compared our current approach with a more straightforward design of the estimation in the mean and variance which is denoted as the RADT-MV (empirical). In RADT-MV (empirical), we directly calculate the mean and variance over the dataset. To be specific, we calculate the return of all the trajectories in the offline dataset and use the mean and variance of these returns to augment the source dataset. The results are shown in the [Figure 8](#). It is clear that our approach RADT-MV leverages the value function as the estimation outperforms the straightforward design of RADT-MV(empirical) in most of the body mass and joint noise settings in HalfCheetah.

6 Conclusion and Future Work

We introduced the Return Augmented Decision Transformer (RADT) method for off-dynamics reinforcement learning which augments the return function of trajectories from the source environment to better align with the target environment. We presented two practical implementations of our method: RADT-DARA, derived from existing dynamic programming reward augmentation techniques, and RADT-MV, which matches the mean and variance of the return function under a Gaussian approximation of the return distribution. Through rigorous theoretical analysis, we showed that RADT when trained only on the source domain’s dataset can achieve the same level of suboptimality as policies learned directly in the target domain. Our extensive experiments in MuJoCo environments demonstrate that RADT outperforms baseline algorithms in off-dynamics RL. This work establishes RADT as a promising method for leveraging source domain data to improve policy learning in target domains with limited data, thus addressing key challenges in offline, off-policy, and off-dynamics RL. Future work could explore extensions and applications of RADT in more diverse RL environments and further refine the augmentation techniques to enhance efficiency and effectiveness.

A Sample Complexity of Off-Dynamics RCSL

In this section, we provide the rigorous analysis of the sample complexity of the off-dynamics RCSL. To this end, we first define some useful notations. We assume there are N^S trajectories in the source dataset \mathcal{D}^S , and N^T trajectories in the target dataset \mathcal{D}^T . Denote P_β^S as the joint distribution of state, action, reward and return-to-go induced by the behavior policy β in the source environment, and P_β^T in the target environment. Denote d_π^S as the marginal distribution of state s induced by any policy π in the source environment, and d_π^T in the target environment.

Denote $J^T(\pi)$ as the expected cumulative reward under any policy π and the target environment. For any return-to-go g in the source dataset \mathcal{D}^S , we transform g by an oracle defined in (4.3) with others remain the same, then we get a modified dataset $\tilde{\mathcal{D}}^S$. We denote the mixed dataset as $\mathcal{D} = \mathcal{D}^T \cup \tilde{\mathcal{D}}^S$.

We first show the sample complexity of DT with only the samples from the target dataset \mathcal{D}^T . If we only use the offline dataset \mathcal{D}^T collect from the target environment, i.e., at training time we minimize the empirical negative log-likelihood loss:

$$\hat{L}^T(\pi) = - \sum_{\tau \in \mathcal{D}^T} \sum_{1 \leq t \leq H} \log \pi(a_t | s_t, g(s_t)).$$

Then we get the following sample complexity guarantee based on the result in [Brandfonbrener et al. \(2022\)](#).

Corollary A.1. There exists a conditioning function $f : \mathcal{S} \rightarrow \mathbb{R}$ such that assumptions (1)-(3) in [Assumption 4.2](#), (1) and (2) in [Assumption 4.3](#) hold. Further assume assumptions (1)-(3) in [Assumption 4.4](#) hold. Then for some $\delta \in (0, 1)$, with probability at least $1 - \delta$, we have

$$J^T(\pi^*) - J^T(\hat{\pi}_f) \leq O\left(\frac{C_f}{\alpha_f} H^2 \left(\sqrt{c} \left(\frac{\log |\Pi| / \delta}{N^T}\right)^{1/4} + \sqrt{\epsilon_{\text{approx}}}\right) + \frac{\epsilon}{\alpha_f} H^2\right).$$

Now we consider the case of mixed dataset, where we train our policy on both the target dataset and the source dataset using the proposed returned conditioned decision transformer methods. Note that the size of the target environment dataset is usually small, while the size of the source environment dataset is much larger, that is, $N^T \ll N^S$. If we incorporate the modified source dataset into the supervised learning, that is, we minimize the following empirical negative log-likelihood loss:

$$\hat{L}^{\text{mix}}(\pi) = - \sum_{\tau \in \mathcal{D}} \sum_{1 \leq t \leq H} \log \pi(a_t | s_t, g(s_t)). \quad (\text{A.1})$$

An observation is that, with the modified source dataset, the regret $J^T(\pi^*) - J^T(\hat{\pi}_f)$ can be significantly reduced. We state this observation in the following theorem, which is the formal version of [Theorem 4.5](#).

Theorem A.2. There exists a conditioning function f such that [Assumptions 4.2](#) and [4.3](#) hold. Further assume [Assumption 4.4](#) holds. Then for some $\delta \in (0, 1)$, with probability at least $1 - \delta$, we have

$$J^T(\pi^*) - J^T(\hat{\pi}_f) \leq O\left(\frac{C_f}{\alpha_f} \frac{N^S + N^T}{N^S / \gamma_f + N^T} H^2 \left(\sqrt{c} \left(\frac{\log |\Pi| / \delta}{N^T + N^S}\right)^{1/4} + \sqrt{\epsilon_{\text{approx}}}\right) + \frac{\epsilon}{\alpha_f} H^2\right). \quad (\text{A.2})$$

Remark A.3. Compared to [Corollary A.1](#), [Theorem A.2](#) suggests that the modified samples from the source domain could enhance the performance of RCSL when the domain occupancy overlap coefficient γ_f is large. In particular, when $N^S \gg N^T$ and $\gamma_f = O(1)$, [\(A.2\)](#) can be simplified to

$$J^T(\pi^*) - J^T(\hat{\pi}_f) \leq O\left(\frac{C_f}{\alpha_f} H^2 \left(\sqrt{c} \left(\frac{\log |\Pi| / \delta}{N^S}\right)^{1/4} + \sqrt{\epsilon_{\text{approx}}}\right) + \frac{\epsilon}{\alpha_f} H^2\right),$$

which significantly improves the bound on suboptimality in [Corollary A.1](#).

B Proof of [Theorem A.2](#)

Lemma B.1 (Corollary 1 of [Brandfonbrener et al. \(2022\)](#)). Under the assumptions in [Assumption 4.2](#), there exists a conditioning function such that

$$J^T(\pi^*) - J^T(\pi_f^{\text{RCSL}}) \leq \epsilon \left(\frac{1}{\alpha_f} + 3\right) H^2.$$

Lemma B.2 (Lemma 1 of [Brandfonbrener et al. \(2022\)](#)). For any two policies π, π' , we have

$$\|d_\pi^T - d_{\pi'}^T\|_1 \leq 2H \cdot \mathbb{E}_{s \sim d_\pi^T} [TV(\pi(\cdot|s) || \hat{\pi}(\cdot|s))].$$

We define $d_\beta^{\text{mix}} = \frac{N^T}{N^T + N^S} d_\beta^T + \frac{N^S}{N^T + N^S} d_\beta^S$. Define

$$L(\hat{\pi}) = \mathbb{E}_{s \sim d_\beta^{\text{mix}}, g \sim P_\beta^T(\cdot|s)} [D_{\text{KL}}(P_\beta^T(\cdot|s, g) || \hat{\pi}(\cdot|s, g))].$$

Theorem B.3. Consider any function $f : \mathcal{S} \rightarrow \mathbb{R}$ such that the assumptions in [Assumption 4.3](#) hold. Then for any estimated RCSL policy $\hat{\pi}$ that conditions on f at test time (denoted by $\hat{\pi}_f$), we have

$$J^T(\pi_f^{\text{RCSL}}) - J^T(\hat{\pi}_f) \leq \frac{C_f \gamma_f}{\alpha_f} H^2 \sqrt{2L(\hat{\pi})}.$$

Proof. By definition and [Lemma B.2](#), we have

$$\begin{aligned} J^T(\pi_f) - J^T(\hat{\pi}_f) &= H(\mathbb{E}_{P_{\pi_f}^T} [r(s, a)] - \mathbb{E}_{P_{\hat{\pi}_f}^T} [r(s, a)]) \\ &\leq H \cdot \|d_{\pi_f} - d_{\hat{\pi}_f}\|_1 \\ &\leq 2 \cdot \mathbb{E}_{s \sim d_{\pi_f}^T} [TV(\pi_f(\cdot|s) || \hat{\pi}_f(\cdot|s))] H^2. \end{aligned}$$

Next, we have

$$\begin{aligned} &2 \cdot \mathbb{E}_{s \sim d_{\pi_f}^T} [TV(\pi_f(\cdot|s) || \hat{\pi}_f(\cdot|s))] \\ &= \mathbb{E}_{s \sim d_{\pi_f}^T} \left[\int_a |P_\beta^T(a|s, f(s)) - \hat{\pi}(a|s, f(s))| \right] \\ &= \mathbb{E}_{s \sim d_{\pi_f}^T} \left[\frac{P_\beta^T(f(s)|s)}{P_\beta^T(f(s)|s)} \int_a |P_\beta^T(a|s, f(s)) - \hat{\pi}(a|s, f(s))| \right] \\ &\leq 2 \frac{C_f}{\alpha_f} \mathbb{E}_{s \sim d_\beta^T, g \sim P_\beta^T(\cdot|s)} [TV(P_\beta^T(a|s, f(s)) || \hat{\pi}(a|s, f(s)))] \end{aligned}$$

$$\begin{aligned}
&\leq 2 \frac{C_f}{\alpha_f} \frac{N^S + N^T}{N^S/\gamma_f + N^T} \cdot \mathbb{E}_{s \sim d_{\beta}^{mix}, g \sim P_{\beta}^T(\cdot|s)} [TV(P_{\beta}^T(a|s, f(s)) || \hat{\pi}(a|s, f(s)))] \\
&\leq \frac{C_f}{\alpha_f} \frac{N^S + N^T}{N^S/\gamma_f + N^T} \cdot \mathbb{E}_{s \sim d_{\beta}^{mix}, g \sim P_{\beta}^T(\cdot|s)} \left[\sqrt{2KL(P_{\beta}^T(a|s, f(s)) || \hat{\pi}(a|s, f(s)))} \right] \\
&\leq \frac{C_f}{\alpha_f} \frac{N^S + N^T}{N^S/\gamma_f + N^T} \sqrt{2L(\hat{\pi})}.
\end{aligned}$$

□

Proof of Theorem A.2. Following the same argument in the proof of Corollary 3 in Brandfonbrener et al. (2022), we have

$$J^T(\pi_f^{\text{RCSL}}) - J^T(\hat{\pi}_f) \leq O\left(2 \frac{C_f}{\alpha_f} \frac{N^S + N^T}{N^S/\gamma_f + N^T} H^2 \left(\sqrt{c} \left(\frac{\log |\Pi|/\delta}{N^S + N^T} \right)^{1/4} + \sqrt{\epsilon_{\text{approx}}} \right)\right).$$

Invoking Lemma B.1, we have

$$J^T(\pi^*) - J^T(\hat{\pi}_f) \leq O\left(2 \frac{C_f}{\alpha_f} \frac{N^S + N^T}{N^S/\gamma_f + N^T} H^2 \left(\sqrt{c} \left(\frac{\log |\Pi|/\delta}{N^T + N^S} \right)^{1/4} + \sqrt{\epsilon_{\text{approx}}} \right) + \frac{\epsilon}{\alpha_f} H^2\right).$$

This completes the proof. □

C Detailed Experiment Setting

C.1 Environment and Dataset

In this section, we provide details of the environments and datasets used in our experiments. We evaluate our approaches in the Hopper, Walker2D, and HalfCheetah environments, using the corresponding environments from Gym as our target environments. For the target datasets, we create two distinct datasets: one with a small amount of data (1T) and another with a large amount of data (10T). The 10T dataset contains ten times the number of trajectories as the 1T dataset.

We employ BodyMass shift, JointNoise shift, Kinematic shift, and Morphology shift to construct the source environments. The following descriptions provide detailed insights into the process of creating these source environments.

- **BodyMass Shift:** Adjust the body mass of the agents. We change the mass of the body in the Gym environment. For detailed body mass settings, refer to Table 4
- **JointNoise Shift:** Introduce noise to the agents' joints. We add the noise to the actions when collecting the source data. For detailed information on the joint noise settings, refer to Table 4.
- **Kinematic shift:**
 - **Walker2D - Broken Right Foot:** The rotation range of the joint on the right leg's foot is modified from $[-45, 45]$ to $[-0.45, 0.45]$. The detailed modifications to the XML file are as follows:

```

1 <joint axis="0 -1 0" name="foot_joint" pos="0 0 0.1" range
   ="-0.45 0.45" type="hinge"/>

```

- **Hopper - Broken Joints:** The rotation range of the joint on the head is modified from $[-150, 0]$ to $[-0.15, 0]$, and the rotation range of the joint on the foot is adjusted from $[-45, 45]$ to $[-18, 18]$. The detailed modifications to the XML file are as follows:

```
1 <joint axis="0 -1 0" name="thigh_joint" pos="0 0 1.05" range
   ="-0.15 0" type="hinge"/>
```

```
1 <joint axis="0 -1 0" name="foot_joint" pos="0 0 0.1" range
   ="-18 18" type="hinge"/>
```

- **HalfCheetah - Broken Back Thigh:** The rotation range of the joint on the thigh of the back leg is modified from $[-0.52, 1.05]$ to $[-0.0052, 0.0105]$. The detailed modifications to the XML file are as follows:

```
1 <joint axis="0 1 0" damping="6" name="bthigh" pos="0 0 0"
   range="-.0052 .0105" stiffness="240" type="hinge"/>
```

- **Morphology Shift:**

- **Walker2D - No Right Thigh:** The size of the right thigh has been adjusted, with the endpoint of the thigh's geometry modified from $0\ 0\ 0.6$ to $0\ 0\ 1.045$, shifting the leg joint's position accordingly from 0.6 to 1.045 along the Z-axis. The starting point of the leg geometry has been updated to $0\ 0\ 1.045$ to align with the new joint position, and the endpoint has been changed from $0\ 0\ 0.1$ to $0\ 0\ 0.3$. The foot's position has been simplified by removing the division $/2$ and moving its Z-axis location from 0.1 to 0 . The foot joint has also been raised from 0.1 to 0.3 , extending the foot geometry along the Z-axis from 0.1 to 0.3 , thereby increasing the length of the foot capsule. The specific modifications to the XML file are as follows:

```
1 <body name="thigh" pos="0 0 1.05">
2   <joint axis="0 -1 0" name="thigh_joint" pos="0 0 1.05"
   range="-150 0" type="hinge"/>
3   <geom friction="0.9" fromto="0 0 1.05 0 0 1.045" name="
   thigh_geom" size="0.05" type="capsule"/>
4   <body name="leg" pos="0 0 0.35">
5     <joint axis="0 -1 0" name="leg_joint" pos="0 0 1.045"
   range="-150 0" type="hinge"/>
6     <geom friction="0.9" fromto="0 0 1.045 0 0 0.3" name
   ="leg_geom" size="0.04" type="capsule"/>
7     <body name="foot" pos="0.2 0 0">
8       <joint axis="0 -1 0" name="foot_joint" pos="0 0
   0.3" range="-45 45" type="hinge"/>
9       <geom friction="0.9" fromto="-0.0 0 0.3 0.2 0
   0.3" name="foot_geom" size="0.06" type="
   capsule"/>
10    </body>
11  </body>
12 </body>
```

- **Hopper - Enlarged Head:** The head size has been modified, and the torso geometry’s radius has been increased from 0.05 to 0.125. This adjustment primarily affects the capsule-shaped geometry, enlarging its size and potentially increasing its thickness in the simulation. The detailed modifications to the XML file are as follows:

```
1 <geom friction="0.9" fromto="0 0 1.45 0 0 1.05" name="
  torso_geom" size="0.125" type="capsule"/>
```

- **HalfCheetah - No Thighs:** The thigh size has been modified, and the geometry has been altered to nearly zero length. The capsule radius remains unchanged keeping 0.046. The detailed modifications to the XML file are as follows:

```
1 <geom fromto ="0 0 0 -0.0001 0 -0.0001" name ="bthigh" size
  ="0.046" type="capsule"/ >
```

```
2 <body name="bshin" pos="-0.0001 0 -0.0001">
```

```
1 <geom fromto ="0 0 0 0.0001 0 0.0001" name ="fthigh" size
  ="0.046" type="capsule"/ >
```

```
2 <body name="fshin" pos="0.0001 0 0.0001">
```

For the source datasets, we employ the BodyMass shift and JointNoise shift datasets from (Liu et al., 2022). The Kinematic Shift and Morphology Shift datasets are collected using the same methodology as in D4RL. Behavior policies are generated by training agents with SAC using rlkit (<https://github.com/vitchyr/rlkit>), with checkpoints used for dataset collection. We collect the Random, Medium, Medium Replay, and Medium Expert datasets, each corresponding to different performance levels based on their respective SAC checkpoints. Table 5 provides details about the SAC checkpoints. Additionally, for the ablation study, we explore different BodyMass and JointNoise shifts compared to those specified in Table 4. We also collect medium-level source datasets for the Hopper, Walker2D, and HalfCheetah environments. For the JointNoise shift setting datasets, instead of training a new SAC policy and using it to collect data through interaction with the environment, we introduce random noise from a specified range directly to the actions.

Table 4 BodyMass Shift and JointNoise Shift in Hopper, Walker2D and HalfCheetah.

	Hopper		Walker2D		HalfCheetah	
	BodyMass	JointNoise	BodyMass	JointNoise	BodyMass	JointNoise
Source	mass[-1]=2.5	action[-1]+noise	mass[-1]=1.47	action[-1]+noise	mass[4]=0.5	action[-1]+noise
Target	mass[-1]=5.0	action[-1]+0	mass[-1]=2.94	action[-1]+0	mass[4]=1.0	action[-1]+0

C.2 Baselines

In our experiments, we select the BEAR (Kumar et al., 2019), AWR (Peng et al., 2019), BCQ (Fujimoto et al., 2019), CQL (Kumar et al., 2020), and MOPO (Yu et al., 2020) and their DARA (Liu et al., 2022) augmented methods as our baselines compared with DT(Chen et al., 2021) and our RADT approaches.

Table 5 SAC performance results in the Medium setting were evaluated across the Walker2D, Hopper, and HalfCheetah environments under BodyMass, Morphology, and Kinematic shift conditions. In the Walker2D environment, the BodyMass shift ranges from 'Mass①' to 'Mass③' corresponding to 'Mass = [0.735, 1.47, 2.25]'. The Morphology shift involves the removal of the right thigh, while the Kinematic shift is characterized by a broken right foot. For the Hopper environment, the BodyMass shift ranges from 'Mass①' to 'Mass③' with 'Mass = [1.25, 3.75, 5]'. The Morphology shift includes an enlarged head, and the Kinematic shift involves broken joints. In the HalfCheetah environment, the BodyMass shift ranges from 'Mass①' to 'Mass③' with 'Mass = [0.25, 0.5, 0.75]'. The Morphology shift corresponds to the removal of both thighs, while the Kinematic shift involves a broken back thigh.

	BodyMass Shift			Morphology Shift	Kinematic Shift
	Mass①	Mass②	Mass③		
Walker2D-Medium	75.848 ± 1.418	76.151 ± 0.677	76.139 ± 0.408	49.585 ± 0.704	71.797 ± 0.677
Hopper-Medium	75.392 ± 2.202	63.516 ± 1.237	48.672 ± 1.259	55.526 ± 1.624	52.892 ± 2.514
HalfCheetah-Medium	41.510 ± 0.241	42.731 ± 0.128	40.079 ± 0.263	40.167 ± 0.236	40.066 ± 0.309

C.3 Hyperparameters

In this section, we detail the hyperparameters used for our RADT methodologies. For RADT approaches, the initial step involves dataset augmentation using either the DARA algorithm or the Direct Matching of Return Distributions technique. Subsequently, the augmented dataset is utilized to train the Decision Transformer (DT), which is then evaluated in the target environment. Specifically, for **RADT-DARA**, the dataset augmentation employs the DARA algorithm, with its corresponding hyperparameters presented in [Table 6](#). For **RADT-MV**, the augmentation process is detailed in [Section 5.3](#), where a well-trained Conservative Q-Learning (CQL) algorithm assesses the state values, implementing clipping to mitigate extreme values. The hyperparameters for CQL training are detailed in [Table 7](#), the clipping technique ratios are displayed in [Table 8](#), and the parameters for DT training are provided in [Table 9](#).

Table 6 Hyperparameters used in the DARA algorithm.

Hyperparameter	Value
SA Discriminator MLP Layers	4
SAS Discriminator MLP Layers	4
Hidden Dimension	256
Nonlinearity Function	ReLU
Optimizer	RMSprop
Batch Size	256
Learning Rate	3×10^{-4}
Δr Coefficient η	0.1

Table 7 Hyperparameters used in the CQL algorithm.

Hyperparameter	Value
Actor MLP Layers	3
Critic MLP Layers	3
Hidden Dimension	256
Nonlinearity Function	ReLU
Optimizer	Adam
Batch size	256
Discount Factor	0.99
Temperature	1.0
Actor Learning rate	1×10^{-4}
Critic Learning rate	3×10^{-4}

D Additional Experiments Results

Due to space limitations in the main text, this section presents more comprehensive experimental results, including additional variance information, and additional experimental results from the HalfCheetah environment.

Table 8 Hyperparameters for the Clipping Technique Employed in the RADT-MV Algorithm.

Dataset	Clipping Ratio
Walker2D Random	$0.9 < \theta < 1.25$
Walker2D Medium	$0.9 < \theta < 2$
Walker2D Medium Replay	$0.9 < \theta < 1.25$
Walker2D Medium Expert	$0.9 < \theta < 1.25$
Hopper Random	$0.9 < \theta < 1$
Hopper Medium	$0.9 < \theta < 1$
Hopper Medium Replay	$0.9 < \theta < 1$
Hopper Medium Expert	$0.9 < \theta < 1$
HalfCheetah Random	$0.67 < \theta < 1.5$
HalfCheetah Medium	$0.67 < \theta < 1.5$
HalfCheetah Medium Replay	$0.67 < \theta < 1.5$
HalfCheetah Medium Expert	$0.67 < \theta < 1.5$

Table 9 Hyperparameters used in the DT algorithm.

Hyperparameter	Value
Transformer Layers	4
Attention Heads	1
Embedding Dimension	128
Nonlinearity Function	ReLU
Batch size	64
Context length K	20
Return-to-go conditioning	[500,1500,2500,3500,4500,5500,6000]
Dropout	0.1
Learning rate	3×10^{-4}

D.1 Additional Experiments in HalfCheetah Environment

We conduct ablation studies in the HalfCheetah environment to verify the effectiveness of the RADT methods. These studies include evaluating the performance of RADT methods under other shift settings in the HalfCheetah environment and assessing the impact of the clipping technique on RADT performance. The experiment results for the two ablation studies are shown in the [Figure 9](#) and [Figure 10](#). In the body mass shift settings, our proposed method RADT-DARA and RADT-MV can both mitigate the off-dynamics problem and the RADT-MV performs better than the RADT-DARA. In the joint noise setting, the RADT-DARA still performs well with the large joint noise. The performance is only inferior to the RADT-DARA and DT in the small joint noise. This phenomenon may be caused by the small dynamics shift and randomness introduced by our augment methods. In the kinematic setting, the performance of our methods remains consistent with the body mass and joint noise setting. In the morphology settings, the RADT-DARA fails, while the RADT-MV still performs well under this hard dynamic shift problem. In the [Figure 10](#), we demonstrate the clip performance in RADT-MV in HalfCheetah. It shows that the clip method can improve the performance and robustness of our method.

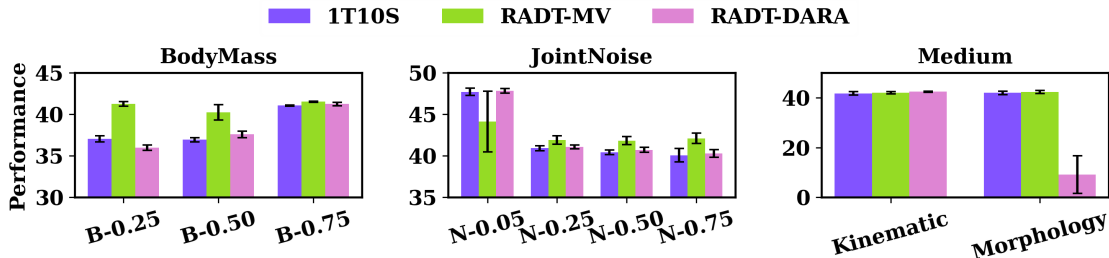


Figure 9 Performance of RADT methods under varying environment shift settings in the HalfCheetah Medium environment. "B-x" denotes that the body mass in the simulator is set to x. "N-x" denotes the addition of random noise in the range (-x, +x) to the action. Refer [Appendix C.1](#) for details about Kinematic and Morphology Shift settings in the Medium HalfCheetah environment.

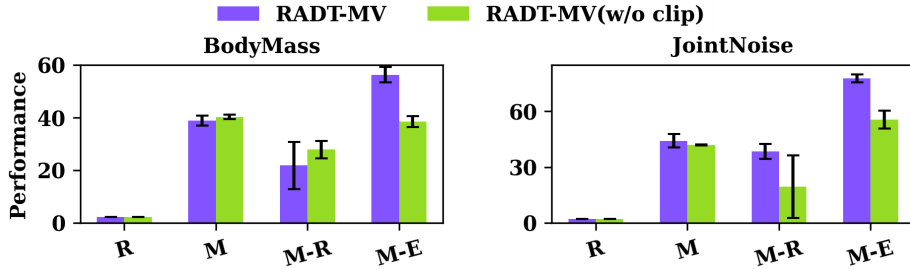


Figure 10 Performance comparison of **RADT-MV** and **RADT-MV without the clipping technique** across BodyMass and JointNoise shift settings in Random(R), Medium(M), Medium-Replay(M-R), and Medium-Expert(M-E) environments in HalfCheetah.

D.2 Complete Experiment Results

In [Table 2](#), we present the partial performance of various algorithms and their DARA variants in the Walker2D and Hopper environments under BodyMass and JointNoise shift settings. The complete experimental results are provided in [Table 10](#).

Additionally, to facilitate an intuitive comparison between our methods and other baselines, we calculate the rank score for each algorithm. Ranks are assigned within each dataset, with the top-performing algorithm receiving rank 1, the second-best rank 2, and so on. In cases of tied scores, algorithms are assigned the same rank, with subsequent ranks adjusted accordingly. The final rank score for each algorithm is calculated by summing its ranks across all datasets, with lower average rank scores indicating superior performance. [Figure 1](#) presents the rank scores for all algorithms, clearly demonstrating that the RADT methods we propose outperform others in most cases.

Table 10 Performance comparison of various algorithms under BodyMass and JointNoise distribution shifts in the Walker2D, Hopper and HalfCheetah environments, using the Random, Medium, Medium Replay and Medium Expert **1T10S** dataset. The **1T10S** dataset comprises a **1T** (target) dataset and a **10S** (source) dataset. "**D-XX**" denotes the DARA-augmented variant of the '**XX**' algorithm.

	BEAR	AWR	BCQ	CQL	MOPO	D-BEAR	D-AWR	D-BCQ	D-CQL	D-MOPO	IT10S-DT	RADT-MV	RADT-DARA
Walker2D Random	BodyMass 2.799 ± 1.609	5.637 ± 0.407	6.074 ± 4.710	7.392 ± 0.117	1.011 ± 3.892	0.899 ± 1.296	6.044 ± 0.265	7.428 ± 2.361	6.857 ± 0.301	0.987 ± 4.394	6.571 ± 4.824	7.318 ± 0.098	7.734 ± 2.886
	JointNoise 3.621 ± 2.768	3.121 ± 4.385	5.566 ± 0.192	6.995 ± 3.120	0.968 ± 1.412	1.757 ± 2.558	6.920 ± 1.348	6.074 ± 1.174	6.074 ± 2.041	2.134 ± 0.748	6.236 ± 5.720	7.657 ± 0.919	6.075 ± 1.914
Walker2D Medium	BodyMass 5.776 ± 1.653	77.449 ± 0.340	70.681 ± 0.539	73.317 ± 1.368	21.617 ± 1.277	6.516 ± 3.220	78.004 ± 0.911	72.023 ± 0.695	74.276 ± 2.582	21.621 ± 1.063	78.768 ± 1.233	80.857 ± 1.715	78.257 ± 2.423
	JointNoise 4.926 ± 1.418	67.636 ± 1.468	62.696 ± 1.037	68.962 ± 0.865	23.552 ± 1.063	6.933 ± 1.884	64.303 ± 0.513	60.681 ± 1.118	69.141 ± 0.944	23.574 ± 0.665	71.068 ± 1.022	72.651 ± 1.834	71.779 ± 1.706
Walker2D Medium Replay	BodyMass 0.0663 ± 4.951	47.033 ± 2.278	50.714 ± 1.918	54.759 ± 0.335	11.563 ± 2.751	1.078 ± 2.083	32.008 ± 1.286	51.447 ± 3.108	57.432 ± 0.764	12.129 ± 2.755	73.064 ± 1.920	73.708 ± 1.570	67.565 ± 0.799
	JointNoise 0.474 ± 0.719	31.023 ± 2.551	50.601 ± 1.611	50.600 ± 1.589	11.379 ± 0.596	0.384 ± 3.823	36.307 ± 2.442	50.714 ± 0.876	51.742 ± 1.061	15.389 ± 0.559	58.253 ± 3.181	55.722 ± 2.653	62.220 ± 0.383
Walker2D Medium Expert	BodyMass 19.799 ± 3.116	110.324 ± 1.053	112.343 ± 1.488	107.187 ± 3.209	18.324 ± 0.708	17.491 ± 2.844	109.749 ± 2.632	113.069 ± 1.602	105.401 ± 2.186	20.714 ± 0.339	84.430 ± 0.823	88.235 ± 1.886	85.328 ± 0.865
	JointNoise 14.225 ± 1.338	104.662 ± 2.370	112.926 ± 1.491	104.019 ± 0.294	17.429 ± 0.639	14.203 ± 1.602	108.915 ± 1.915	111.249 ± 1.092	108.230 ± 1.206	19.325 ± 3.119	115.746 ± 1.116	111.06 ± 2.247	111.236 ± 0.914
Hopper Random	BodyMass 4.474 ± 1.404	5.164 ± 3.802	18.843 ± 1.199	9.418 ± 4.581	4.141 ± 0.951	6.561 ± 1.956	6.976 ± 1.252	19.212 ± 2.876	8.745 ± 0.917	4.144 ± 0.493	8.746 ± 0.554	9.668 ± 0.054	8.467 ± 1.196
	JointNoise 5.156 ± 5.194	7.922 ± 0.654	14.458 ± 2.481	9.460 ± 0.948	4.139 ± 1.808	4.054 ± 0.445	6.716 ± 0.388	18.843 ± 0.346	10.286 ± 1.278	5.872 ± 0.736	6.236 ± 1.352	7.524 ± 0.656	7.842 ± 0.149
Hopper Medium	BodyMass 22.436 ± 0.103	25.843 ± 0.325	24.853 ± 1.615	49.094 ± 2.207	20.765 ± 3.350	25.608 ± 1.063	26.594 ± 1.267	26.487 ± 1.366	45.101 ± 0.342	21.495 ± 0.848	34.057 ± 0.177	39.435 ± 1.239	37.787 ± 1.914
	JointNoise 8.536 ± 1.965	57.021 ± 0.938	74.559 ± 0.605	71.495 ± 0.126	23.556 ± 1.327	10.576 ± 2.052	61.463 ± 0.702	74.853 ± 0.626	63.611 ± 1.136	24.992 ± 0.944	70.685 ± 0.796	70.356 ± 3.657	78.325 ± 2.522
Hopper Medium Replay	BodyMass 6.282 ± 0.132	55.607 ± 2.310	64.519 ± 0.813	66.455 ± 0.636	5.594 ± 1.701	2.619 ± 0.128	44.883 ± 1.595	64.168 ± 0.291	68.163 ± 0.559	5.482 ± 1.061	64.216 ± 1.504	66.092 ± 0.233	60.393 ± 1.086
	JointNoise 1.841 ± 3.814	37.821 ± 1.205	65.103 ± 0.703	61.302 ± 1.207	5.498 ± 0.568	5.637 ± 0.291	63.937 ± 3.879	64.519 ± 1.102	63.178 ± 1.218	6.147 ± 0.157	61.870 ± 0.249	77.825 ± 1.638	83.525 ± 1.728
Hopper Medium Expert	BodyMass 22.934 ± 3.022	57.595 ± 0.612	109.367 ± 0.834	70.467 ± 2.712	30.541 ± 3.616	31.090 ± 0.463	78.202 ± 0.239	110.014 ± 2.153	72.140 ± 1.934	30.540 ± 0.842	33.554 ± 0.846	52.873 ± 0.454	33.631 ± 1.605
	JointNoise 39.031 ± 1.079	74.708 ± 1.889	108.639 ± 2.028	72.512 ± 0.781	30.537 ± 0.842	33.052 ± 0.385	60.952 ± 0.879	111.587 ± 1.602	94.128 ± 1.213	32.589 ± 1.985	108.254 ± 1.583	109.367 ± 1.084	108.261 ± 2.612
HalfCheetah Random	BodyMass 24.424 ± 0.307	2.348 ± 0.099	2.248 ± 0.001	19.745 ± 0.694	30.140 ± 0.765	25.547 ± 0.287	2.355 ± 0.168	2.248 ± 0.001	20.242 ± 0.521	25.160 ± 2.135	2.205 ± 0.014	2.220 ± 0.021	2.309 ± 0.018
	JointNoise 28.838 ± 0.239	2.790 ± 0.146	2.248 ± 0.001	21.089 ± 0.648	32.439 ± 0.404	26.146 ± 0.215	2.205 ± 0.047	2.246 ± 0.001	26.309 ± 0.561	27.514 ± 0.404	2.215 ± 0.011	2.206 ± 0.015	2.210 ± 0.014
HalfCheetah Medium	BodyMass 5.431 ± 1.518	42.293 ± 0.862	39.835 ± 0.427	37.081 ± 0.358	58.457 ± 1.449	6.009 ± 1.705	41.800 ± 0.830	39.333 ± 0.506	37.189 ± 0.218	59.311 ± 0.949	36.954 ± 0.260	40.250 ± 0.911	37.599 ± 0.395
	JointNoise 1.948 ± 1.058	41.992 ± 0.762	50.511 ± 0.371	49.046 ± 0.420	61.073 ± 0.315	2.901 ± 0.402	42.545 ± 0.731	52.149 ± 0.437	49.284 ± 0.570	61.447 ± 0.734	47.725 ± 0.431	44.149 ± 3.672	47.833 ± 0.284
HalfCheetah Medium Replay	BodyMass 7.425 ± 1.307	15.088 ± 5.339	32.553 ± 1.258	37.508 ± 0.520	50.429 ± 1.306	4.909 ± 0.562	17.918 ± 3.701	32.095 ± 1.258	37.721 ± 0.440	52.600 ± 0.621	20.966 ± 9.607	27.812 ± 3.256	24.059 ± 2.271
	JointNoise 18.337 ± 0.498	31.742 ± 4.199	46.567 ± 2.563	51.560 ± 0.246	51.918 ± 1.584	17.929 ± 0.479	38.125 ± 1.775	49.066 ± 0.645	52.991 ± 0.438	51.258 ± 1.709	36.509 ± 4.414	38.417 ± 4.068	38.031 ± 3.529
HalfCheetah Medium Expert	BodyMass 4.356 ± 0.431	88.155 ± 1.836	61.7713 ± 4.610	61.104 ± 4.131	51.040 ± 4.461	2.948 ± 0.691	89.201 ± 2.419	63.465 ± 3.303	62.665 ± 5.326	56.616 ± 2.609	54.981 ± 1.147	56.228 ± 2.930	51.357 ± 8.231
	JointNoise 3.195 ± 0.391	88.647 ± 2.669	62.486 ± 10.025	84.099 ± 11.109	54.630 ± 10.104	8.789 ± 0.271	89.220 ± 1.800	71.007 ± 4.201	84.210 ± 0.506	60.014 ± 7.011	70.573 ± 8.599	77.762 ± 2.009	77.751 ± 2.702

References

- BHARGAVA, P., CHITNIS, R., GERAMIFARD, A., SODHANI, S. and ZHANG, A. (2024). When should we prefer decision transformers for offline reinforcement learning? In *The Twelfth International Conference on Learning Representations*.
URL <https://openreview.net/forum?id=vpV7f0FQy4> (p. 10.)
- BRANDFONBRENER, D., BIETTI, A., BUCKMAN, J., LAROCHE, R. and BRUNA, J. (2022). When does return-conditioned supervised learning work for offline reinforcement learning? *Advances in Neural Information Processing Systems* **35** 1542–1553. (pp. 2, 3, 6, 7, 16, 17, and 18.)
- CHEN, L., LU, K., RAJESWARAN, A., LEE, K., GROVER, A., LASKIN, M., ABBEEL, P., SRINIVAS, A. and MORDATCH, I. (2021). Decision transformer: Reinforcement learning via sequence modeling. *Advances in neural information processing systems* **34** 15084–15097. (pp. 2, 3, 4, and 20.)
- EMMONS, S., EYSENBACH, B., KOSTRIKOV, I. and LEVINE, S. (2021). Rvs: What is essential for offline rl via supervised learning? *arXiv preprint arXiv:2112.10751* . (pp. 2 and 3.)
- EYSENBACH, B., ASAWA, S., CHAUDHARI, S., LEVINE, S. and SALAKHUTDINOV, R. (2020). Off-dynamics reinforcement learning: Training for transfer with domain classifiers. *arXiv preprint arXiv:2006.13916* . (pp. 1, 2, 3, 4, and 5.)
- FU, J., KUMAR, A., NACHUM, O., TUCKER, G. and LEVINE, S. (2020). D4rl: Datasets for deep data-driven reinforcement learning. *arXiv preprint arXiv:2004.07219* . (p. 8.)
- FUJIMOTO, S., MEGER, D. and PRECUP, D. (2019). Off-policy deep reinforcement learning without exploration. In *International conference on machine learning*. PMLR. (pp. 9 and 20.)
- JIANG, Y., ZHANG, T., HO, D., BAI, Y., LIU, C. K., LEVINE, S. and TAN, J. (2021). Simgan: Hybrid simulator identification for domain adaptation via adversarial reinforcement learning. In *2021 IEEE International Conference on Robotics and Automation (ICRA)*. IEEE. (p. 1.)
- KUMAR, A., FU, J., SOH, M., TUCKER, G. and LEVINE, S. (2019). Stabilizing off-policy q-learning via bootstrapping error reduction. *Advances in neural information processing systems* **32**. (pp. 9 and 20.)
- KUMAR, A., ZHOU, A., TUCKER, G. and LEVINE, S. (2020). Conservative q-learning for offline reinforcement learning. *Advances in Neural Information Processing Systems* **33** 1179–1191. (pp. 9 and 20.)
- LABER, E. B., MEYER, N. J., REICH, B. J., PACIFICI, K., COLLAZO, J. A. and DRAKE, J. M. (2018). Optimal treatment allocations in space and time for on-line control of an emerging infectious disease. *Journal of the Royal Statistical Society Series C: Applied Statistics* **67** 743–789. (p. 1.)
- LEVINE, S. (2018). Reinforcement learning and control as probabilistic inference: Tutorial and review. *arXiv preprint arXiv:1805.00909* . (p. 5.)
- LEVINE, S., KUMAR, A., TUCKER, G. and FU, J. (2020). Offline reinforcement learning: Tutorial, review, and perspectives on open problems. *arXiv preprint arXiv:2005.01643* . (p. 2.)

- LIU, J., ZHANG, H. and WANG, D. (2022). Dara: Dynamics-aware reward augmentation in offline reinforcement learning. *arXiv preprint arXiv:2203.06662* . (pp. **1**, **2**, **3**, **4**, **9**, **11**, and **20**.)
- LIU, Z., CLIFTON, J., LABER, E. B., DRAKE, J. and FANG, E. X. (2023). Deep spatial q-learning for infectious disease control. *Journal of Agricultural, Biological and Environmental Statistics* **28** 749–773. (p. **1**.)
- LIU, Z. and XU, P. (2024). Distributionally robust off-dynamics reinforcement learning: Provable efficiency with linear function approximation. In *International Conference on Artificial Intelligence and Statistics*. PMLR. (p. **1**.)
- PAN, S. J. and YANG, Q. (2009). A survey on transfer learning. *IEEE Transactions on knowledge and data engineering* **22** 1345–1359. (p. **3**.)
- PAN, X., YOU, Y., WANG, Z. and LU, C. (2017). Virtual to real reinforcement learning for autonomous driving. *arXiv preprint arXiv:1704.03952* . (p. **1**.)
- PENG, X. B., KUMAR, A., ZHANG, G. and LEVINE, S. (2019). Advantage-weighted regression: Simple and scalable off-policy reinforcement learning. *arXiv preprint arXiv:1910.00177* . (pp. **9** and **20**.)
- VASWANI, A., SHAZEER, N., PARMAR, N., USZKOREIT, J., JONES, L., GOMEZ, A. N., KAISER, Ł. and POLOSUKHIN, I. (2017). Attention is all you need. *Advances in neural information processing systems* **30**. (p. **4**.)
- XU, M., SHEN, Y., ZHANG, S., LU, Y., ZHAO, D., TENENBAUM, J. and GAN, C. (2022). Prompting decision transformer for few-shot policy generalization. In *international conference on machine learning*. PMLR. (p. **3**.)
- YU, T., THOMAS, G., YU, L., ERMON, S., ZOU, J. Y., LEVINE, S., FINN, C. and MA, T. (2020). Mopo: Model-based offline policy optimization. *Advances in Neural Information Processing Systems* **33** 14129–14142. (pp. **9** and **20**.)
- ZHENG, Q., ZHANG, A. and GROVER, A. (2022). Online decision transformer. In *international conference on machine learning*. PMLR. (p. **3**.)
- ZHUANG, Z., PENG, D., ZHANG, Z., WANG, D. ET AL. (2024). Reinformer: Max-return sequence modeling for offline rl. *arXiv preprint arXiv:2405.08740* . (p. **4**.)